Research Article | Vol. 25, No. 15 | 24 Jul 2017 | OPTICS EXPRESS 17004
Optics EXPRESS

Hadamard circular masks: high focal depth with high throughput

L. LEDESMA-CARRILLO,[1] C. M. GÓMEZ-SARABIA,[2] M. TORRES-CISNEROS,[1] R. GUZMÁN-CABRERA,[3] C. GUZMÁN-CANO,[1] AND J. OJEDA-CASTAÑEDA[1,*]

[1]*Electronics Department, DICS, University of Guanajuato, 36885 Salamanca, Guanajuato, Mexico*
[2]*Digital Arts, DICS, University of Guanajuato, 36885 Salamanca, Guanajuato, Mexico*
[3]*Electrical Engineering, DICS, University of Guanajuato, 36885 Salamanca, Guanajuato, Mexico*
**jojedacas@ugto.mx*

Abstract: We present a class of binary masks that encode, in polar coordinates, the values of a Hadamard matrix of order N. For order N ≥ 2, the binary masks increase the Strehl ratio vs. focus error by the factor N, with the highest possible light throughput. Since a Strehl ratio with high tolerance to defocus does not guarantee a modulation transfer function (MTF) with low sensitivity to focus errors, then, we show that for N = 16 the binary mask reduces also the impact of focus error on the MTF. Equivalently, the discrete binary mask has Fisher information with low variations to defocus.

OCIS codes: (100.0100) Image processing; (110.0110) Imaging systems; (050.1220) Apertures; (070.6110) Spatial filtering; (100.1390) Binary phase-only filters; (110.4850) Optical transfer functions.

References

1. N. J. A. Sloane, T. Fine, P. G. Phillips, and M. Harwit, "Codes for multiplex spectrometry," Appl. Opt. **8**(10), 2103–2106 (1969).
2. M. Harwit and N. J. A. Sloane, *Hadamard Transform Optics* (Academic, 1979)
3. M. E. Gehm, S. T. McCain, N. P. Pitsianis, D. J. Brady, P. Potuluri, and M. E. Sullivan, "Static two-dimensional aperture coding for multimodal, multiplex spectroscopy," Appl. Opt. **45**(13), 2965–2974 (2006).
4. R. Raskar, A. Agrawal, and J. Tumblin, "Coded exposure photography: motion deblurring via fluttered shutter," in *Proceedings SIGGRAPH '06 795* (ACM, 2006), paper 804.
5. S. S. Gorthi, D. Schaak, and E. Schonbrun, "Fluorescence imaging of flowing cells using a temporally coded excitation," Opt. Express **21**(4), 5164–5170 (2013).
6. E. Tajahuerce, V. Durán, P. Clemente, E. Irles, F. Soldevila, P. Andrés, and J. Lancis, "Image transmission through dynamic scattering media by single-pixel photodetection," Opt. Express **22**(14), 16945–16955 (2014).
7. F. Soldevila, E. Salvador-Balaguer, P. Clemente, E. Tajahuerce, and J. Lancis, "High-resolution adaptive imaging with a single photodiode," Sci. Rep. **5**(1), 14300 (2015).
8. J. H. McLeod, "Axicon: a new type of optical element," J. Opt. Soc. Am. **44**(8), 592–597 (1954).
9. M. Rioux, R. Tremblay, and P. A. Bélanger, "Linear, annular, and radial focusing with axicons and applications to laser machining," Appl. Opt. **17**(10), 1532–1536 (1978).
10. N. Davidson, A. A. Friesem, and E. Hasman, "Holographic axilens: high resolution and long focal depth," Opt. Lett. **16**(7), 523–525 (1991).
11. J. Ojeda-Castañeda, S. Ledesma, and C. M. Gómez-Sarabia, "Tunable apodizers and tunable focalizers using helical pairs," Photonics Lett. Pol. **5**(1), 20–22 (2013).
12. C. W. McCutchen, "Generalized aperture and the three-dimensional diffraction image," J. Opt. Soc. Am. **54**(2), 240 (1964).
13. J. Ojeda-Castañeda, L. R. Berriel-Valdos, and E. Montes, "Bessel annular apodizers: imaging characteristics," Appl. Opt. **26**(14), 2770–2772 (1987).
14. J. Ojeda-Castañeda and L. R. Valdós, "Arbitrarily high focal depth with finite apertures," Opt. Lett. **13**(3), 183–185 (1988).
15. J. Ojeda-Castañeda and L. R. Berriel-Valdos, "Zone plate for arbitrarily high focal depth," Appl. Opt. **29**(7), 994–997 (1990).
16. J. Ojeda-Castañeda, P. Andrés, and M. Martínez-Corral, "Zone plates with cells apodized by Legendre profiles," Appl. Opt. **29**(9), 1299–1303 (1990).
17. Q. Cao and J. Jahns, "Modified Fresnel zone plates that produce sharp Gaussian focal spots," J. Opt. Soc. Am. A **20**(8), 1576–1581 (2003).
18. A. W. Lohmann, J. Ojeda-Castañeda, and A. Serrano-Heredia, "Synthesis of analog apodizers with binary angular sectors," Appl. Opt. **34**(2), 317–322 (1995).

#293095 https://doi.org/10.1364/OE.25.017004
Journal © 2017 Received 21 Apr 2017; revised 5 Jul 2017; accepted 5 Jul 2017; published 10 Jul 2017

Optics EXPRESS

19. J. Ojeda-Castañeda, P. Andrés, and M. Martínez-Corral, "Zero axial irradiance by annular screens with angular variation," Appl. Opt. **31**(22), 4600–4602 (1992).
20. L. Ledesma-Carrillo, R. Guzmán-Cabrera, C. M. Gómez-Sarabia, M. Torres-Cisneros, and J. Ojeda-Castañeda, "Tunable field depth: hyperbolic optical masks," Appl. Opt. **56**(1), A104–A114 (2017).
21. G. Häusler, "A method to increase the depth of focus by two step image processing," Opt. Commun. **6**(1), 38–42 (1972).
22. J. Ojeda-Castaneda, R. Ramos, and A. Noyola-Isgleas, "High focal depth by apodization and digital restoration," Appl. Opt. **27**(12), 2583–2586 (1988).
23. W. Chi and N. George, "Electronic imaging using a logarithmic asphere," J. Opt. Soc. Am. A **20**(12), 2260 (2003).
24. X. Gao, Z. Fei, W. Xu, and F. Gan, "Tunable three-dimensional intensity distribution by a pure phase-shifting apodizer," Appl. Opt. **44**(23), 4870–4873 (2005).
25. J. Ojeda-Castañeda, J. E. A. Landgrave, and C. M. Gómez-Sarabia, "Conjugate phase plate use in analysis of the frequency response of imaging systems designed for extended depth of field," Appl. Opt. **47**(22), E99–E105 (2008).
26. M. Demenikov, G. Muyo, and A. R. Harvey, "Experimental demonstration of continuously variable optical encoding in a hybrid imaging system," Opt. Lett. **35**(12), 2100–2102 (2010).
27. J. Ojeda-Castañeda and C. M. Gómez-Sarabia, "Tuning field depth at high resolution by pupil engineering," Adv. Opt. Photonics **7**(4), 814–880 (2015).
28. T. M. Cover and J. A. Thomas, *Elements of Information Theory* (Wiley, 1991).
29. L. L. Scharf, *Statistical Signal Processing* (Addison-Wesley, 1991).
30. E. R. Dowski, Jr. and W. T. Cathey, "Extended depth of field through wave-front coding," Appl. Opt. **34**(11), 1859–1866 (1995).
31. M. Demenikov and A. R. Harvey, "Parametric blind-deconvolution algorithm to remove image artifacts in hybrid imaging systems," Opt. Express **18**(17), 18035–18040 (2010).

1. Introduction

Rectangular masks encoded with Hadamard matrices are useful for increasing the light gathering power of optical spectrometers [1–3]. They are also useful for reducing the impact of motion blur and of focus errors by coding the exposure time of imaging devices [4], as well as for temporally coding fluorescence excitations [5]. Rather recently, rectangular masks encoding Hadamard matrices were used for gathering images with a single pixel detector [6, 7].

The classical optical element for producing long axial irradiance distribution is the axicon and its related devices [8–11]. Among several approaches for beam shaping, it is convenient to recognize that one can apply McCutchen theorem [12], for relating (in terms of a 1-D Fourier transform) the axial irradiance distribution with certain representations of the pupil functions [13, 14].

This later approach helps to identify zone plates [15–17], and other nonconventional masks for spreading the axial irradiance distribution [18]. One of these nonconventional masks can sustain a dark spot along the optical axis [19].

However, it is relevant to recognize the following. If an optical device spreads well the irradiance distribution along the optical axis, the device is not necessarily useful for imaging extended objects, with low sensitivity to focus errors. The converse is also true. If an optical device has a modulation transfer functions (MTF) with low sensitivity to focus errors; the device does not necessarily concentrate the maximum irradiance on-axis [20].

Here our aim is to present a new class of binary, circular masks that encode Hadamard matrices. At certain regions, the amplitude transmittance is unity. And at the Babinet complementary regions, the amplitude transmittance is equal to minus one.

Typically, for reducing the impact to focus on the MTF, the masks have continuous complex amplitude transmittances. See for example references [21–26], and a rather recent review [27].

To the best of our knowledge, the current paper is the first report on the use of binary masks that are able to do two different jobs: (a) to extend at will the axial irradiance distribution; (b) to increase the depth of field of an imaging device that gathers pictures with moderate spatial frequency content. Hence, even when it is possible to make comparisons

Optics EXPRESS

with other methods for extending field depth, the proposed masks belong to a different category.

In what follows, we show that the proposed binary masks, of order $N \geq 2$, can increase the Strehl ratio vs. focus error by the factor N, with the highest possible light throughput. Furthermore, one member of the class (N = 16) generates a MTF with reduced sensitivity to defocus. We show that this binary mask preserves the area under the MTF, despite the presence of focus errors.

As an alternative method for evaluating the performance of the proposed device, we report numerical evaluations on the behavior of the Fisher information [28, 29] with focus error. We show that this binary mask has Fisher information with low variations to defocus. The latter figure of merit was first proposed by Dowski and Cathey, for evaluating the behavior of a cubic phase filter [30].

Even when our mathematical model uses the properties of the Hadamard matrices, our proposal does not dwell on code information theory.

To our end, as depicted schematically in Fig. 1, the values along the lines of a Hadamard matrix are used for encoding the equiangular segments of the proposed masks. Additionally, the values along the columns of a Hadamard matrix are used for encoding disks that are spaced with the quadratic value of the radius.

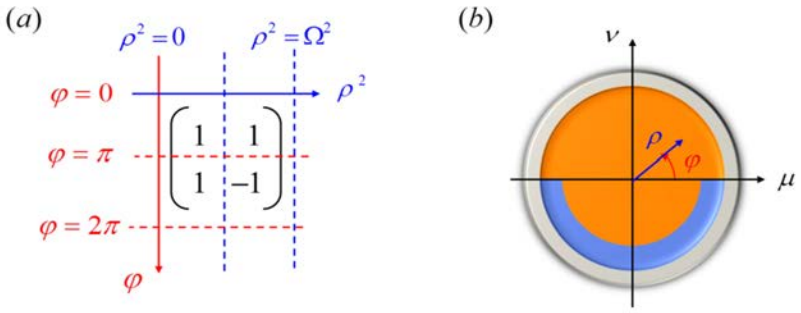

Fig. 1. Geometrical strategy for implementing a circular version of a Hadamard mask of order N = 2: In (a), we show a pseudo-Cartesian display, to be discussed in section 3. In (b) we use polar coordinates for showing the circular Hadamard mask of order N = 2. We render in orange the regions where the amplitude transmittance is equal to unity. And in blue, we depict the regions where the amplitude transmittance has a phase delay of π.

By using McCutchen theorem, we show that the axial irradiance distribution is well spread along the optical axis. If you will, the Strehl ratio vs focus error is scaled up. Furthermore, for validating our proposal, we evaluate numerically some images for showing that one Hadamard circular mask can extend field depth, when gathering images of scenes with moderate frequency content.

In section 2, we discuss the basic theory for relating the complex amplitude transmittance of the masks with the axial irradiance distribution. In section 3, we discuss the procedure used for mapping the values of the Hadamard matrices in complex amplitude transmittance of equiangular segments and square spaced radial disks. We show that the proposed masks are useful for simultaneously implementing the high focal depth of a small pupil aperture, and the light gathering power of a large pupil aperture. In section 4, we evaluate the modulation transfer function (MTF), as well as the area under the MTF of the proposed masks. Equivalently, we show that one member of the new class of mask has Fisher information with low variations to defocus. We report also images depicting the extension of field depth.

2. Axial irradiance distribution

As is shown in Fig. 2, in the paraxial regime, the 3-D complex amplitude point spread function, $p(r, \theta, z)$ is obtained by evaluating the following integral

Optics EXPRESS

$$p(r,\theta,z)=\int_0^{\Omega}\int_0^{2\pi} P(\rho,\varphi)\exp\left\{i2\pi\left[-\frac{\lambda z}{2}\rho^2+r\rho\cos(\theta-\varphi)\right]\right\}\rho\, d\rho\, d\varphi. \quad (1)$$

In Eq. (1) the polar coordinates at the Fraunhofer plane are (ρ, φ); and we denote as P(ρ, φ) the complex amplitude transmittance of the proposed masks.

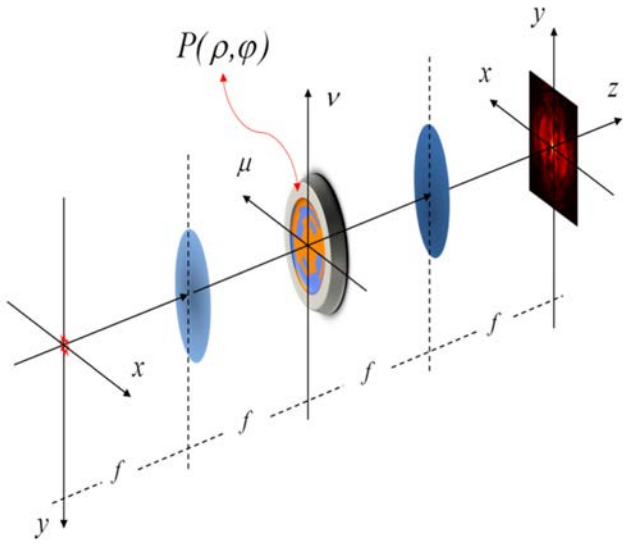

Fig. 2. Schematics of a classical optical processor. At the Fraunhofer plane we locate a circular Hadamard mask (of order N = 8) for generating the irradiance impulse response.

By setting r = 0 in Eq. (1), we can obtain the complex amplitude distribution along the optical axis. Here, we express the axial complex amplitude distribution as

$$p(0,\theta,z)=2\pi\int_0^{\Omega}\left\{\frac{1}{2\pi}\int_0^{2\pi} P(\rho,\varphi)\, d\varphi\right\}\exp\left\{i2\pi\left[-\frac{\lambda z}{2}\rho^2\right]\right\}\rho\, d\rho. \quad (2)$$

Next, aiming to apply McCutchen theorem, it is convenient to employ the following change of variables

$$\zeta=\left(\frac{\rho}{\Omega}\right)^2-\frac{1}{2};\quad Q(\zeta,\varphi)=P(\rho,\varphi). \quad (3)$$

$$\langle Q(\zeta)\rangle=\frac{1}{2\pi}\int_0^{2\pi} Q(\zeta,\varphi)\, d\varphi=\frac{1}{2\pi}\int_0^{2\pi} P(\rho,\varphi)\, d\varphi.$$

In Eq. (3) we denote the angular average of the circular masks as < Q(ζ) >. In Fig. 3, we show that the change of variables in Eq. (3) can be thought of as performing a nonlinear, geometrical mapping from a circular aperture to a rectangular window, or vice versa.

Optics EXPRESS

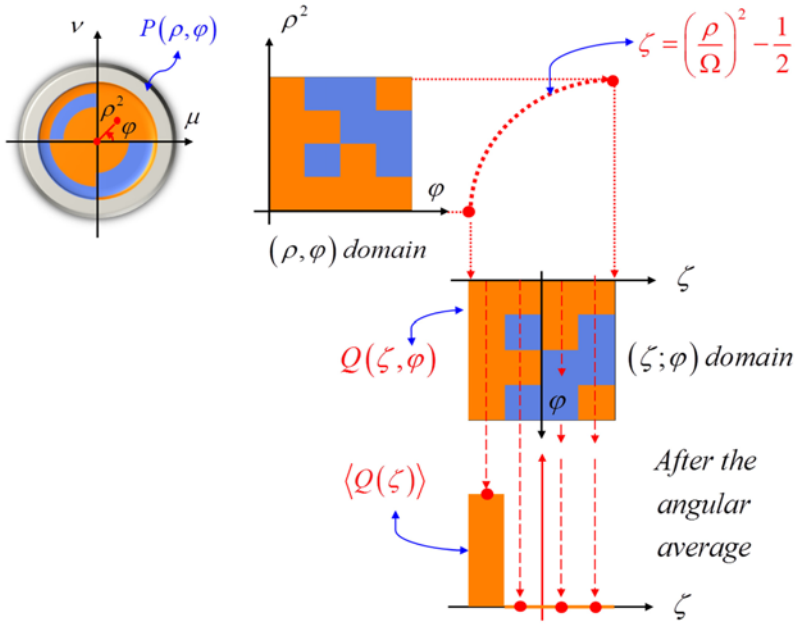

Fig. 3. Schematics illustrating, in a clockwise route, the change of variables describe in Eq. (3).

By using the variables in Eq. (3), we rewrite Eq. (2) as follows

$$p(0,\theta,z)=(\pi\Omega^2)\exp\left(-i\frac{\pi}{2}\lambda\Omega^2 z\right)\int_{-\frac{1}{2}}^{\frac{1}{2}}\langle Q(\zeta)\rangle\exp\left[(-i\,\pi\lambda\Omega^2 z)\zeta\right]d\zeta. \quad (4)$$

The result in Eq. (4) is applied next to obtain the Strehl ratio for focus errors. To this end, we relate the axial coordinate z with the wavefront aberration coefficient $W_{2,0}$

$$W_{2,0}=-\frac{\lambda^2\Omega^2}{2}z;\quad q\left(\frac{W_{2,0}}{\lambda}\right)=p(0,\theta,z). \quad (5)$$

Hence, now Eq. (2) reads

$$q\left(\frac{W_{2,0}}{\lambda}\right)=(\pi\,\Omega^2)\exp\left(i\pi\frac{W_{2,0}}{\lambda}\right)\int_{-\frac{1}{2}}^{\frac{1}{2}}\langle Q(\zeta)\rangle\exp\left[i\,2\pi\left(\frac{W_{2,0}}{\lambda}\right)\zeta\right]d\zeta. \quad (6)$$

The normalized irradiance distribution along the optical axis (denoted as the Strehl ratio vs focus errors) is

$$s(W_{2,0})=\frac{\left|q\left(\frac{W_{2,0}}{\lambda}\right)\right|^2}{|q(0)|^2}. \quad (7)$$

Equivalently, by substituting Eq. (6) in Eq. (7), the Strehl ratio vs focus errors reads

Optics EXPRESS

$$s\left(W_{2,0}\right)=\frac{\left|\int_{-\frac{1}{2}}^{\frac{1}{2}}\left\langle Q(\zeta)\right\rangle \exp\left[i2\pi\left(\frac{W_{2,0}}{\lambda}\right)\zeta\right]d\zeta\right|^{2}}{\left|\int_{-\frac{1}{2}}^{\frac{1}{2}}\left\langle Q(\zeta)\right\rangle d\zeta\right|^{2}}. \tag{8}$$

In the next section, we apply Eq. (8) for evaluating the influence that the proposed masks have on the Strehl ratio vs focus errors.

3. Equiangular segments and square distributed radial disks

For coding the proposed masks, we employ a circular support that is represented by the circular function

$$circ\left(\frac{\rho}{\Omega}\right)=\begin{cases}1 & if \quad \rho\le\Omega\\ 0 & if \quad \rho>\Omega\end{cases}. \tag{9}$$

Next, we split the support in N equiangular segments. Hence, at the m-th segment, the angular variations are contained in the interval

$$\left(\frac{m-1}{N}\right)2\pi\le\varphi\le\left(\frac{m}{N}\right)2\pi;\quad m=1,2,3,...N. \tag{10}$$

We also divide the circular support in N, quadratically separated disks. At the n-th disk, the radial variations are contained in the interval

$$\left(\frac{n-1}{N}\right)\Omega^{2}\le\rho^{2}\le\left(\frac{n}{N}\right)\Omega^{2};\quad n=1,2,3,...N. \tag{11}$$

We note that by considering the change of variables in Eq. (3), the radial intervals become rectangular intervals in the dimensionless variable ζ. That is,

$$-\frac{1}{2}+\left(\frac{n-1}{N}\right)\le\zeta\le-\frac{1}{2}+\left(\frac{n}{N}\right);\quad n=1,2,3,...N. \tag{12}$$

Now, by employing Eqs. (10) and (11), we can express the complex amplitude transmittance of the circular Hadamard masks as

$$P\left(\rho,\varphi\right)=\sum_{m=1}^{N}\sum_{n=1}^{N}\ H_{m,n}(N)\ rect\left(\frac{\varphi-\frac{\pi}{N}(2m-1)}{\frac{2\pi}{N}}\right)\ rect\left(\frac{\rho^{2}-\frac{\Omega^{2}}{2N}(2n-1)}{\frac{\Omega^{2}}{N}}\right)circ\left(\frac{\rho}{\Omega}\right). \tag{13}$$

In Eq. (13) the capital letter $H_{m,n}(N)$ denotes the values of the Hadamard matrix of order N. In Fig. 4, we show several members of the novel family of circular Hadamard masks.

Optics EXPRESS

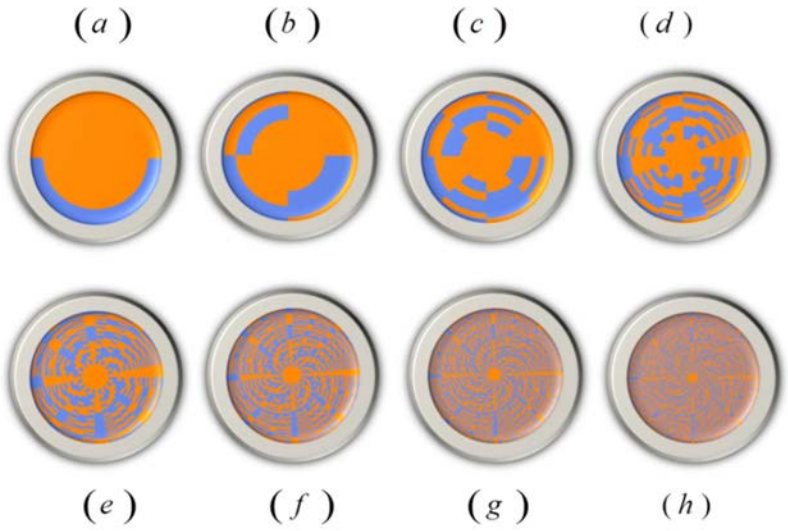

Fig. 4. Display of the circular Hadamard masks of order: (a) N = 2; (b) N = 4; (c) N = 8; (d) N = 16; (e) N = 32; (f) N = 64; (g) N = 128; and (h) N = 256. We render in orange the regions that have complex amplitude transmittances equal to unity; and we render in blue, the regions where there is a phase delay equal to π.

Once that the circular masks are properly specified in the (ρ, φ) domain, we proceed to identify the complex amplitude transmittances in the (ζ, φ) domain. By employing Eqs. (10) and (12), we obtain that in the (ζ, φ) domain, the complex amplitude transmittance is

$$Q(\zeta,\varphi)=\sum_{m=1}^{N}\sum_{n=1}^{N} H_{m,n}\, rect\left(\frac{\varphi-\frac{\pi}{N}(2m-1)}{\frac{2\pi}{N}}\right) rect\left(\frac{\zeta+\frac{1}{2}-\frac{(2n-1)}{2N}}{\frac{1}{N}}\right). \quad (14)$$

In Fig. 5, we show the schematics of the proposed Hadamard masks in the (ζ, φ) domain.

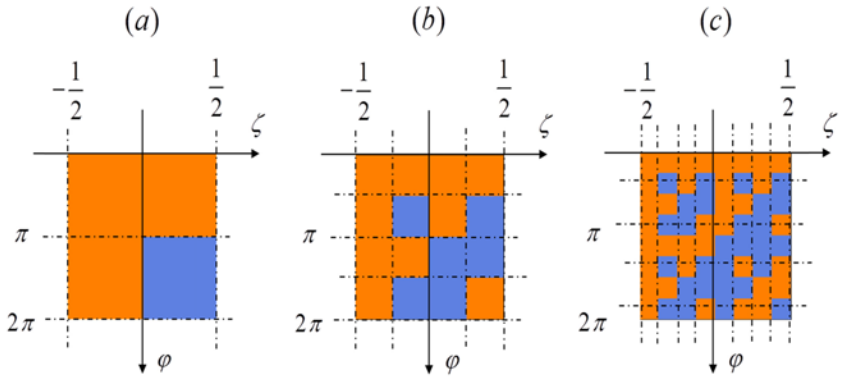

Fig. 5. The circular Hadamard masks are distributed in (ζ, φ) domain as rectangular partitions, which encode the values of a Hadamard matrix of order N: In (a) N = 2; in (b) N = 4; and in (c) N = 8.

Next, we obtain the formula that describes the complex amplitude transmittance, after performing the angular average in the last line of Eq. (3). That is

Optics EXPRESS

$$\left\langle Q(\zeta)\right\rangle = \sum_{n=1}^{N} \left\{ \frac{1}{N} \sum_{m=1}^{N} H_{m,n} \right\} rect\left(\frac{\zeta + \frac{1}{2} - \frac{(2n-1)}{2N}}{\frac{1}{N}} \right). \tag{15}$$

In the Appendix, we show that performing the angular average is equivalent to averaging the columns of a Hadamard matrix. By doing so, one obtains the following Kronecker delta

$$\frac{1}{N} \sum_{m=1}^{N} H_{m,n} = \left\{ \begin{matrix} 1 & If & n=1 \\ 0 & If & n \neq 1 \end{matrix} \right\} = \delta_{n,1}. \tag{16}$$

By using the result in Eq. (16), we can write Eq. (15) as follows

$$\left\langle Q(\zeta)\right\rangle = rect\left(\frac{\zeta + \frac{1}{2} - \frac{1}{2N}}{\frac{1}{N}} \right). \tag{17}$$

And consequently, from Eqs. (8) and (17) we have that

$$s\left(W_{2,0}\right) = \frac{\left| \int_{-\frac{1}{2}}^{-\frac{1}{2}+\frac{1}{N}} \exp\left[i 2\pi \left(\frac{W_{2,0}}{\lambda} \right) \zeta \right] d\zeta \right|^2}{\frac{1}{N^2}}. \tag{18}$$

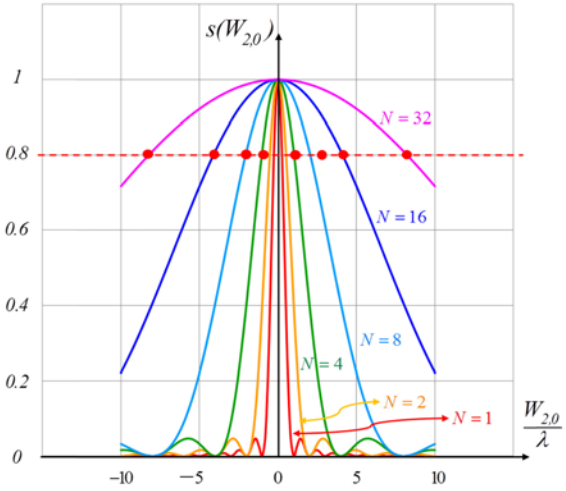

Fig. 6. Variations of the Strehl ratio vs focus error for different circular Hadamard masks. The broken red line, along the horizontal axis, marks the tolerance criterion due to Rayleigh. As the order N of the circular mask increases, the tolerance to focus error is well beyond the value $W_{2,0} \leq \lambda / 4$.

Or equivalently, the Strehl ratio vs focus errors reads

$$s\left(W_{2,0}\right) = \mathrm{sinc}^2\left(\frac{W_{2,0}}{N\,\lambda} \right) \tag{19}$$

Optics EXPRESS

From Eq. (19) we note that by using the circular Hadamard mask of order N, the normalized axial irradiance distribution is scaled up by the factor N; as is depicted in Fig. 6. In other words, the classical Rayleigh tolerance criteria changes to

$$s\left(W_{2,0}\right) \geq 0.8; \qquad if \qquad W_{2,0} \leq N\frac{\lambda}{4} \tag{20}$$

In other words, from the viewpoint of the Strehl ratio vs focus error, the tolerance to focus errors is increased by the factor N. Thus, in principle, by selecting properly the order of the circular Hadamard mask, one can increase focal depth at will the factor N. However, as depicted in Fig. 7, for orders higher than N = 32, the irradiance impulse response is scattered through the image plane. This may be a limitation for imaging devices. Beyond our present scope, due to the scattering characteristics, one may consider using these masks as optical diffusers.

Next, in Fig. 7 we show the numerical evaluations of the irradiance PSF. For obtaining these images, we use the numerical values of Eq. (13) for evaluating Eq. (1), which is of course the amplitude PSF. After this process, we evaluate the square modulus for reporting the irradiance PSF.

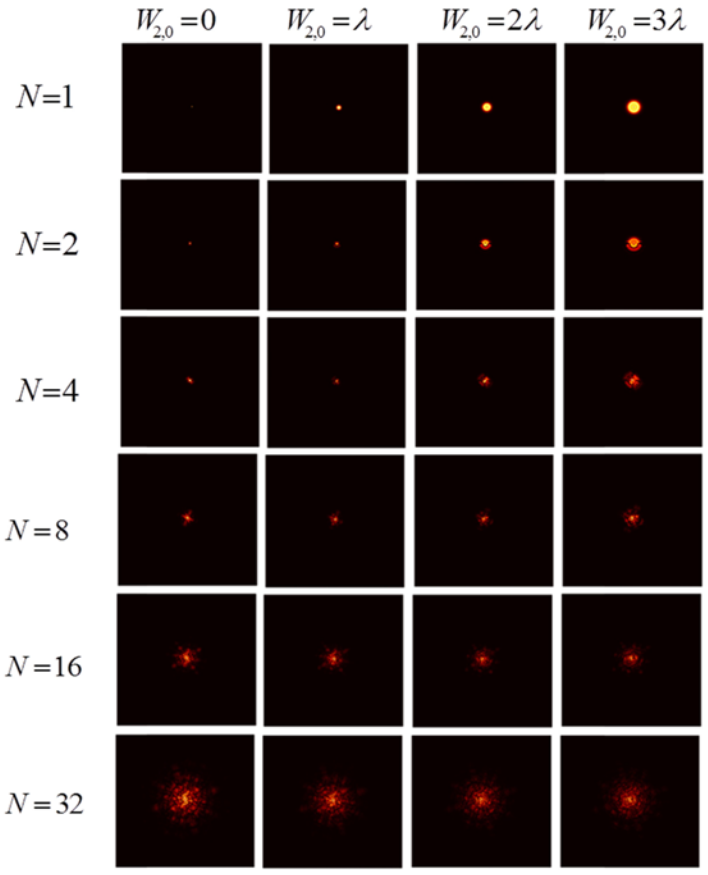

Fig. 7. Irradiance point spread functions (PSF) of the circular Hadamard masks of order N = 1, 2, 4, 8, 16 and 32. Along the columns we vary the focus error coefficient. We note that the PSF do not exhibit circular symmetry, if the order N is greater than 2. We note that for the orders N = 16 and N = 32 the PSF does not change substantially with focus errors.

Optics EXPRESS

The above results are not sufficient, of course, for claiming that the proposed masks can extend field depth. To this later purpose, we require to evaluate the variations of the modulation transfer function (MTF) with focus error, as we report next.

4. Modulation Transfer function and Out-of-Focus Images

Once that the values of the irradiance impulse response are known, then one can obtain the values of the modulation transfer function (MTF), which are shown in Fig. 8.

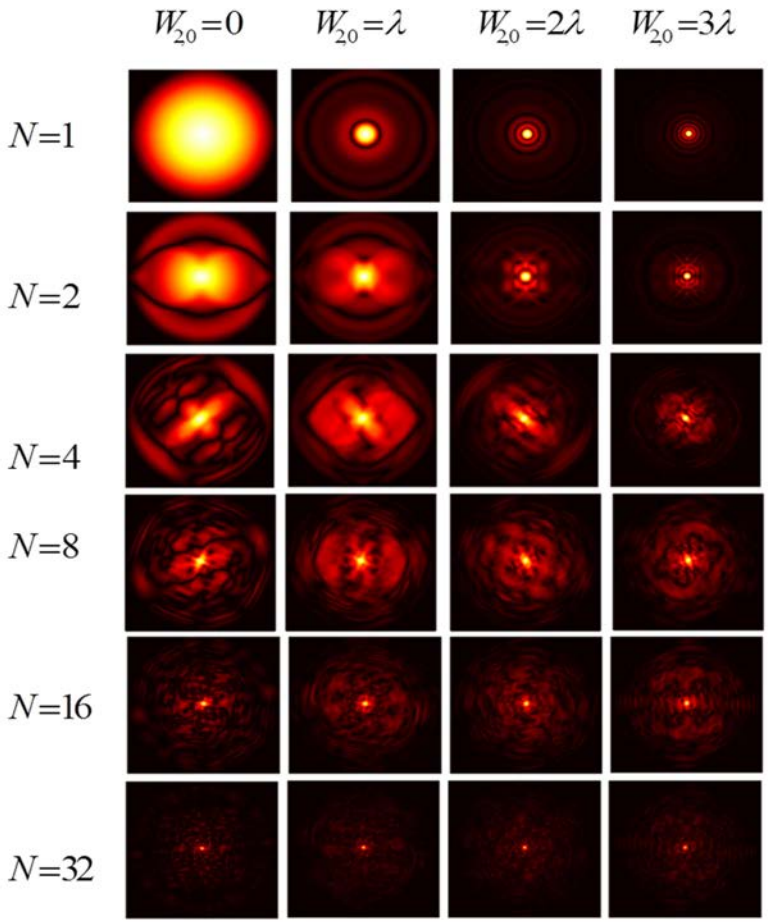

Fig. 8. Display of the Modulation Transfer Function (MTF) of the circular Hadamard masks of order N = 1, 2, 4, 16, and 32; for three values of the focus error coefficient. As in Fig. 7, the MTF does no exhibit circular symmetry; and for the order N = 16 and 32 the MTF does not change substantially with focus errors. However, at high spatial frequencies, the MTF changes substantially with focus error. Consequently, the use of the Hadamard mask is limited to inputs with moderate spatial frequency content.

It is apparent from Fig. 8 that for the circular Hadamard masks of order N = 16 and N = 32, the MTF does not varies substantially; when the optical system suffers from focus errors. From this simple observation, we consider the possibility of using a circular Hadamard mask for extending field depth.

In Fig. 9 we show the numerical evaluations of the MTF for four values of the focus error coefficient. In Fig. 9(a), the graphs display the influence of focus error on the clear pupil aperture. In Fig. 9(b) we show the variations of the MTF, along the horizontal axis ($\theta = 0$) of the circular Hadamard mask of order N = 16.

Optics EXPRESS

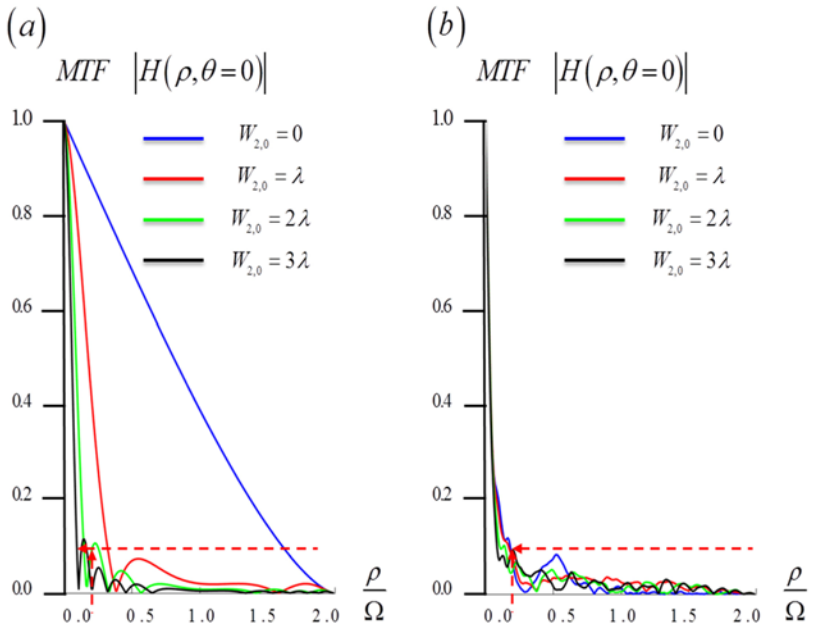

Fig. 9. Graphs depicting the influence of focus error on the Modulation Transfer Function (MTF): In (a) the MTF of a clear pupil aperture. The MTF varies substantially with focus errors. In (b) the MTF (evaluated along the horizontal axis, $\theta = 0$) of the circular Hadamard mask of order $N = 16$. In the range $0 \le \rho \le \Omega / 5$, the MTF has values above a noise level of 10%. In the same range, the MTF does not vary substantially with focus error. However, beyond the selected range of spatial frequencies, the MTF changes wildly with focus error. Then, the usefulness of the Hadamard mask is limited to inputs with moderate spatial frequency content.

It is apparent from Fig. 9(b) that inside the interval $0 \le \rho \le \Omega /5$, the MTF has values greater than one tenth. For many practical applications, a MTF with a threshold above 1/10 is above the noise level. Furthermore, inside the interval $0 \le \rho \le \Omega /5$, we recognize that the values of the MTF remain fairly equal under the influence of focus error. For quantitative evaluation of this later statement, in Fig. 10 we evaluate the areas under the MTFs that are depicted in Fig. 9(b).

For making other useful comparisons, in what follows we show some images that are obtained without and with the circular Hadamard masks.

Optics EXPRESS

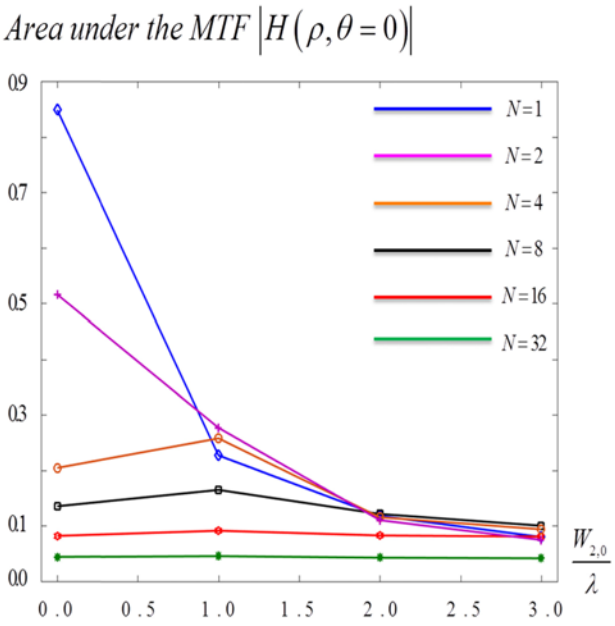

Fig. 10. Graphs showing the variation of the area under the MTF as the focus error coefficient changes from zero to $W_{2,0} = 3\ \lambda$; for the circular Hadamard masks of order N = 1, 2, 4, 8, 16, 32. Even when the values of the area have small values for the orders N = 16 and 32, the area under the MTF remains fairly constant with focus error. These numerical evaluations validate the heuristic considerations in Figs. 6, 7, 8 and 9(b).

As an alternative method for estimating the performance of the Hadamard mask, for extending field depth, we evaluate numerically the Fisher information

$$J\left(W_{2,0}\right) = \int_{\mu=-2\Omega}^{2\Omega} \left| \frac{\partial}{\partial W_{2,0}} H\left(\mu; W_{2,0}\right) \right|^2 d\mu; \qquad 0 \le \left|W_{2,0}\right| \le 3\lambda. \tag{21}$$

In Eq. (21) we denote the optical transfer function vs. focus error as $H(\mu; W_{2,0})$. The function $J(W_{2,0})$ defines the Fisher information of the optical transfer function with variable focus error coefficient $W_{2,0}$. If the Fisher information varies slowly with the coefficient $W_{2,0}$, then the focus error have a low influence on the optical transfer function. In Fig. 11 we plot the Fisher information (in dB) for three different pupil functions.

Optics EXPRESS

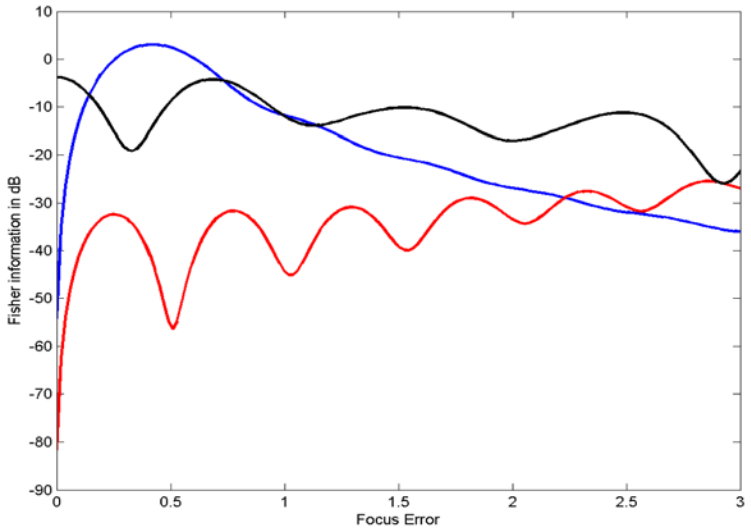

Fig. 11. Fisher information (in dB) as a function of the focus error coefficient. In blue the Fisher information of the clear pupil; in red the Fisher information of the cubic phase mask; and in black the Fisher information of the circular Hadamard mask of order N = 16.

It is apparent from Fig. 11 that, from the viewpoint of the Fisher information, the Hadamard circular mask performs better than the other two pupil functions. However, for visualizing the limitations of the Hadamard circular masks, in what follows we discuss other tests.

It is common to visualize the performance of the masks increasing field focal depth, by looking at the visibility of spoke patterns for different amounts of focus errors. Along line (a) of Fig. 12, we show the out-of-focus images, which are obtained if the optical has a clear pupil aperture. If you will for the Hadamard circular masks of order N = 1. Along line (b) of Fig. 12, we illustrate the efforts from improving the defocused images by using a simple inverse filter. Comparisons between the lines of Fig. 12 illustrate the need of using other methods that extend field depth.

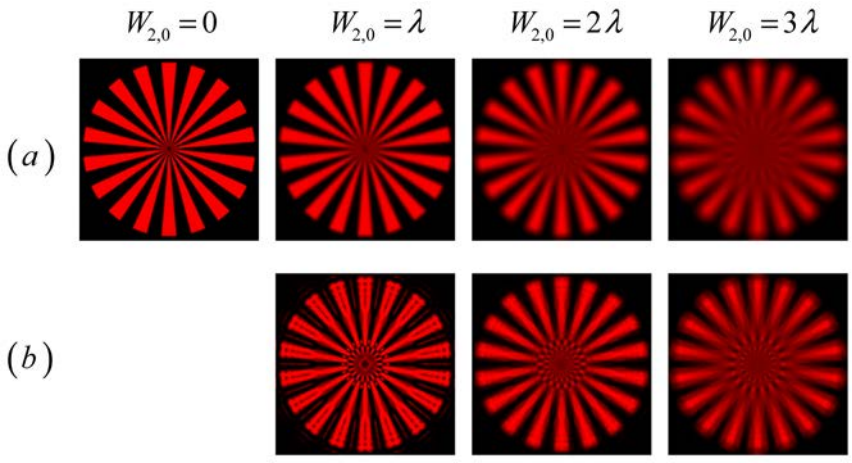

Fig. 12. Images obtained when using a clear pupil aperture, N = 1: Along line (a) we show the in-focus image as well as the defocused images; along line (b) we display the images obtained when using an inverse filter for reconstructing the images along the line (a).

Optics EXPRESS

Now, in Fig. 13 along line (a), we show the numerical simulations of the defocused images, which are obtained when using the circular Hadamard masks of order N = 16. Also in Fig. 13, along line (b), we display the reconstruction of the defocused images, if one uses a simple inverse filter.

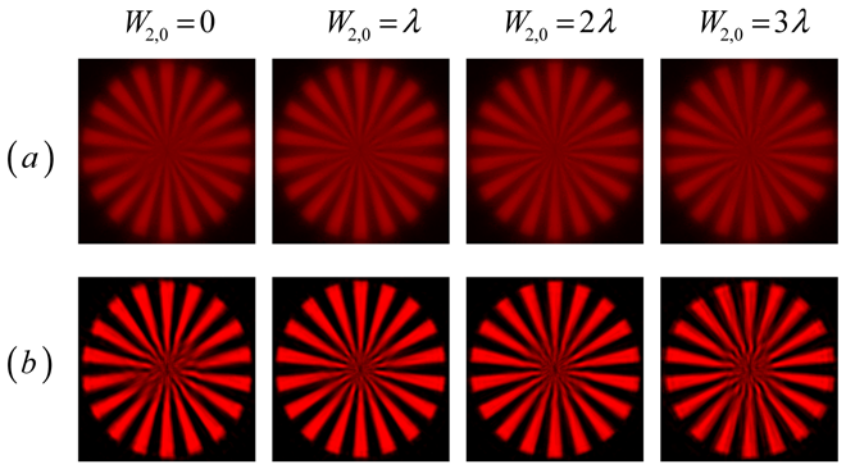

Fig. 13. Images obtained when using a circular Hadamard mask of order N = 16: (a) In-focus image and defocused images; (b) digital reconstruction when using an inverse filter.

From Fig. 13, it is relevant to recognize that despite extending field depth, the Hadamard mask introduces geometrical distortions at high frequencies. This limitation is in agreement with the results shown in Figs. 9 and 10. Hence, the usefulness of the Hadamard mask for extending filed depth is limited to images with moderate spatial frequency content. It is interesting, yet outside our present scope, to explore the possibilities of generating an algorithm that corrects the geometrical distortions at high spatial frequencies, along the lines described in reference [31].

Despite the above limitation, we believe that the outcome in Fig. 13 is a remarkable result, considering that the proposed Hadamard masks are binary filters.

Since one seldom takes pictures of a spoke pattern, it is relevant to perform similar numerical evaluations with a proper picture. To this end, in Fig. 14 along line (a), we show the numerical evaluations of the in-focus and the out-of-focus images of a baboon. Along the second line of Fig. 14, we note that the reconstructed images exhibit artifact noise.

Optics EXPRESS

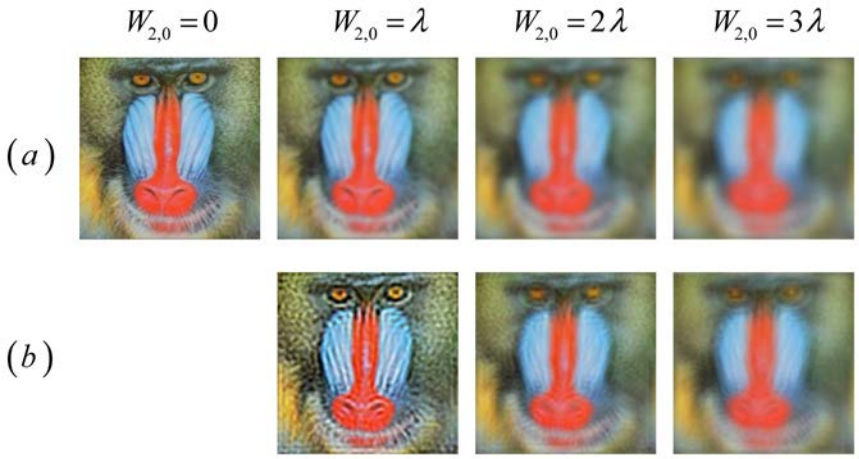

Fig. 14. Baboon images obtained when using a clear pupil aperture. Along line (a) we show the in-focus image as well as the defocused images; along line (b) we display the images obtained when using an inverse filter for reconstructing the images along the line (a).

On the other hand, in Fig. 15 we show the numerical simulations of the defocused images, which are obtained when using the circular Hadamard masks of order N = 16. Along the first line of Fig. 15, we note that the image quality is "democratically" distributed in the out-of-focus plane. Along the second line of Fig. 15, along line (b), we display the reconstruction of the defocused images, if one uses a simple inverse filter, which is set by assuming that the value of the focus error coefficient equal to (3/2)λ.

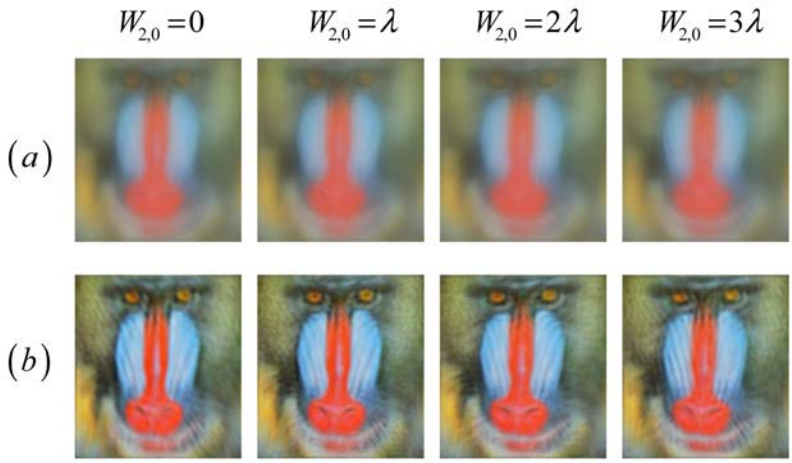

Fig. 15. Baboon images generated when using a circular Hadamard mask of order N = 16 and an inverse, digital post-processing filter. Along line (a) the in-focus and defocused images; along line (b) the digital reconstructions when using an inverse filter that is set at $W_{2,0} = (3/2)\lambda$.

From the second line in Fig. 15, we note that the proposed binary mask renders images of acceptable quality, even in the presence of focus errors. This is a remarkable result, considering that the circular Hadamard mask is a binary filter, which introduces geometrical distortions at high frequencies.

As with other methods for extending field depth, we do require of a two-stage process. In a pre-processing stage the masks reduce the impact of focus errors on the MTF. And at the second stage, the recorded image requires the use of a digital post-processing filter, which reconstructs the initial image modulations.

Optics EXPRESS

5. Conclusions

We have unveiled a family set of phase-only masks that increases, by a factor N, the Strehl ratio to focus error. In other words, we have shown that, from the viewpoint of the axial irradiance distribution, these masks scale up the Rayleigh tolerance to focus error by the factor N.

The new class of optical screens is denoted as circular Hadamard masks. We have described the steps for designing these transparent masks. Specifically, we have indicated that each member of the class is composed by N equiangular segments and by N disks that are spaced with the quadratic value of the radius.

Hence, the mask has N x N elements, whose complex amplitude transmittance is equal to the values of the Hadamard matrix of order N.

For several values of the focus error coefficient, we have evaluated the 2-D irradiance impulse response that is generated by these novel masks. Due to the inherent nonsymmetrical design, the 2-D point spread functions do not exhibit radial symmetry. From these numerical evaluations, we have identified that for the orders N = 16 and N = 32 the irradiance impulse response changes slowly as the focus error varies in the interval $0 \le W_{2,0} \le 3\ \lambda$.

We have stated that to the best of our knowledge, our proposal is the first report on the use of binary masks that are able to do two different jobs: to extend at will the axial irradiance distribution; and to increase the depth of field of an imaging device. Hence, we have claimed that the proposed masks belong to a new category of spatial filters.

We have indicated that, from the viewpoint of the Fisher information, the Hadamard circular mask performs better than both the clear pupil aperture and the cubic phase masks.

We have shown that for the masks, of order N = 16 and N = 32, their modulation transfer function changes slowly with focus error. We have evaluated numerically images for demonstrating that these specific masks can extend the depth of field. However, these binary masks introduce geometrical distortions at high spatial frequencies. Thus, these binary masks are useful only if the input scenes have moderate spatial frequency content.

We have indicated that for orders higher than N = 16, the circular Hadamard masks may be useful as diffusers.

Appendix

In the main text, as Eq. (16), we use the following projection property

$$\frac{1}{N}\sum_{m=1}^{N} H_{m,n} = \left\{ \begin{matrix} 1 & If & n=1 \\ 0 & If & n\neq 1 \end{matrix} \right\} = \delta_{n,1} \tag{22}$$

By construction, we associate Eq. (22) to an angular average operation. We recognize that the order N does not increase in a linear fashion, Hence, for proving Eq. (22), it is not possible to employ a standard, mathematical induction process. In what follows, we employ a heuristic recursive procedure.

We start by noticing that the Hadamard matrix of order N = 1 has only one line and one column; that is H(1) = [1]. Trivially, Eq. (22) is valid for this case. For order N = 2, it is convenient to express the Hadamard matrix as the following direct product

$$H(2) = \begin{bmatrix} H(1) & H(1) \\ H(1) & -H(1) \end{bmatrix} = \begin{bmatrix} 1 & 1 \\ 1 & -1 \end{bmatrix} \tag{23}$$

Then, by adding along the columns of Eq. (23), we obtain

$$\frac{1}{2}\sum_{m=1}^{2} H_{m,n}(2) = \left\{ \begin{matrix} 1 & If & n=1 \\ 0 & If & n=2 \end{matrix} \right\} \tag{24}$$

Optics EXPRESS

Now, for order N = 4, it is convenient again to express the Hadamard matrix as the direct product

$$H(4)=\begin{bmatrix} H(2) & H(2) \\ H(2) & -H(2) \end{bmatrix} \tag{25}$$

We recognize again that by adding along the columns of Eq. (25), we have

$$\frac{1}{4}\sum_{m=1}^{4} H_{m,n}(4)=\begin{Bmatrix} \sum_{m=1}^{4} H_{m,n}(2) & if \quad n=1,2 \\ 0 & if \quad n=3,4 \end{Bmatrix} \tag{26}$$

From Eqs. (25) and (26) we obtain

$$\frac{1}{4}\sum_{m=1}^{4} H_{m,n}(4)=\begin{Bmatrix} 1 & if \quad n=1 \\ 0 & if \quad n=2,3,4 \end{Bmatrix} \tag{27}$$

The above procedure can be repeated for N = 8. Now the direct product is

$$H(8)=\begin{bmatrix} H(4) & H(4) \\ H(4) & -H(4) \end{bmatrix} \tag{28}$$

Now, again by adding along the columns the matrices, we have

$$\frac{1}{8}\sum_{m=1}^{8} H_{m,n}(8)=\begin{Bmatrix} \sum_{m=1}^{8} H_{m,n}(4) & if \quad n=1,2,3,4 \\ 0 & if \quad n=5,6,7,8 \end{Bmatrix} \tag{29}$$

By substituting Eq. (28) in Eq. (29) we obtain

$$\frac{1}{8}\sum_{m=1}^{8} H_{m,n}(8)=\begin{Bmatrix} 1 & if \quad n=1 \\ 0 & if \quad n=2,3,4,5,6,7,8 \end{Bmatrix} \tag{30}$$

From the above results, we claim that it is possible to proceed in the same manner for orders N > 8.